



BIOSYNTHESIS AND ANTIBACTERIAL EVALUATION OF ZINC OXIDE NANOPARTICLES FROM ONION EXTRACT (*ALLIUM CEPA*)

Mona Khamis, Gamal A. Gouda* and Adham M. Nagiub

Department of Chemistry, Faculty of Science, Al-Azhar University, Assiut 71524, Egypt

*The aim of this research is to use red onion extract (*Allium cepa*) in the green synthesis of zinc oxide nanoparticles (ZnO NPs). With an average crystal size of 8.13 nm, X-ray diffraction (XRD) scanning was used to determine the hexagonal wurtzite structure of the ZnO NPs. Infrared spectra (FT-IR) provided evidence of capping and biogenesis stability of ZnO NPs. The absorption peak at 374 nm with an energy gap of 3.32 eV was determined by surface plasmon resonance via UV-visible analysis. Morphological analysis was performed, and the results demonstrated the formation of spherical ZnO NPs with sizes ranging from 2.83 to 15.35 nm. The great purity, intensity, and crystal width of zinc and oxygen was determined by EDS. When compared to a common antibiotic such as ciprofloxacin, which was used as a positive control in the inhibitory zone, ZnO NPs showed more antibacterial effect against *E. coli* than *S. aureus* bacteria. Onion extract and DMSO were added to the control wells, but these additions did not produce an inhibitory zone that could be seen.*

Keywords: Green synthesis, Nanoparticles, TEM, EDX, Antimicrobial activity

INTRODUCTION

Green nanotechnology focuses on the use of non-toxic compounds at mild process conditions to fabricate nanomaterials, thereby, enhancing the environmental sustainability of the nanoparticles¹. This field has gained attention because of the promising features such as eco friendliness^{2&3}, low-costs⁴⁻⁶, simple processes, and relatively high energy savings^{2,7}. Nanomaterials are produced through extensive chemical and physical processes, yet their use and disposal raise concerns about potential environmental impacts. Because of this, biogenic synthesis, often known as a "green synthesis strategy," provides a workable foundation for the long-term and sustainable production of nanomaterials^{8,9}. The plants are eco-friendly¹⁰, sustainable¹¹, free of chemical contamination, less expensive¹², and can be used for mass production^{13,14}. Furthermore presence of various compounds, such as proteins, alkaloids, flavonoids, reducing sugars, polyphenols, etc., in the biomaterials act as reducing and capping agents for the synthesis of NPs from its metal salt precursors¹⁵.

Phytochemical profile of the onion extract is mainly derived from the carbohydrate, lipid, protein, and polyphenols moieties, also quercetin and quercetin 4'-O- β -glucopyranoside were involved in the formation of metal oxide nanoparticles¹⁶. An effective antioxidant and anticancer is the onion (*Allium cepa*)¹⁷. The extract works as a powerful chelating agent to help with the formation of ZnO NPs, because it contains anthocyanins (derivatives of cyanidin) and flavanols¹⁸. Recently, a biological ZnO NPs synthesis based on plant extracts has been established, and it offers several advantages over chemical and physical ways, including lower costs, simpler handling, nontoxicity, and environmental friendliness. ZnO NPs has previously been produced using a variety of plants, including *Citrus sinensis*, *Moringa oleifera*, oak fruit, and *Brassica oleracea*¹⁹. The employing of ZnO NPs in several applications, antibacterial treatment²⁰, solar cells²¹⁻²³, luminous materials²⁰, and drug-delivery²⁴, has generated significant attention.

Here, an environmentally friendly technique for creating ZnO NPs using onion extract has been developed. After that, different

approaches for physicochemical characterization were used to aid in the nanoscale biogenesis of ZnO NPs. In addition, both Gram-positive and Gram-negative bacteria were used to compare the antibacterial capabilities of ZnO NPs to those of ciprofloxacin.

Experimental

Compounds of analytical grade were used in this experiment. Acetonitrile, ethanol, 99 % pure ZnSO₄, 99 % pure NaOH (Scharlau, Spain), HPLC grade from LOBA CHEMIE, and NH₄OH at a concentration of 35% (Merck, UK). Ciprofloxacin was kindly donated by Organo for Pharmaceutical and Chemical Industries in Obour City, Egypt, serving as an antibacterial standard.

Green synthesis of ZnO NPs

With use of distilled water, the red onions were meticulously washed before being shade-dried for about 100 g at room temperature. A glass tank containing the dried onions is filled with 50 % aqueous ethanol and let to soak for 2.5 days. After the solid material has been eliminated and filtered, any leftover solids are subsequently eliminated using Whatman filters. Until it was time to employ the filtrate for the biosynthesis of ZnO NPs, it was kept at 25 °C. At 60 °C, 100 mL of the onion extract solution was gradually added to 60 mM of aqueous ZnSO₄. The pH is adjusted to 10.5 with a 25 % ammonia solution while the mixture is kept at 60 °C and continuously stirred. After the addition, the solution was allowed to react for an hour, at which point a brown precipitate could be seen. After being allowed to rest for 24 hrs, the precipitate was rinsed with double-distilled water and ethanol, and then it was separated by centrifuging at 5000 rpm for 20 minutes. At 60 °C, the material was dried for 6 hrs. ZnO NPs separated precipitate was calcined for 2 hrs at 400 °C²⁵.

Characterizations

To analyze the ZnO NPs crystal phase data, the German Electric Muffle Furnace ST-1200°C-666 was used to produce solid ZnO at the nanoscale. X-ray diffractometer (Philips, PW-1710) was used to determine the ZnO NPs diameters, which ranged from 10 to 80° in 2θ. The size of ZnO NPs was established using Scherers formula and the lattice parameters^{16,26}. Scanning electron microscopy (SEM;

QUANTAFEG-250 with energy-dispersive x-ray spectroscopy; EDX) and transmission electron microscope (TEM; JEM-100CXII, at a voltage of 80 kV) was evaluate ZnO NPs surface morphology. Elemental analysis of the as-prepared NPs was assessed using EDX analysis. The FT-IR spectra of prepared NPs were captured by a Thermo Fishers Nicolet iS10 FT-IR spectrometer. UV-Vis absorption spectra were measured using a Perkin Elmer Spectrophotometer (Lambda 750 UV/Vis/NIR) in 200-900 nm range. On the Hitachi (F-7100) fluorescence spectrophotometer, photoluminescence (PL) measurements were made. Using a micro-Raman Horiba Jobin Yvon LabRam spectrometer, Raman analysis was carried out (HR800).

Antimicrobial activity

In the current work, antimicrobial efficacy of biosynthetic ZnO NPs against various microbes was investigated using the well diffusion method²⁷. The microorganisms used for the antibacterial activity were *Escherichia coli* ATCC 25922, *Salmonella typhimurium* ATCC 14028, *Staphylococcus aureus* ATCC 25923, and *Enterococcus faecalis* ATCC 29212. Ciprofloxacin was the antibacterial agent applied as a positive control. The four distinct ZnO NPs concentrations 225, 250, 275, and 300 µg/mL were made. All the bacteria were tested using different concentrations in DMSO in a 25 µL volume. The experiments were next conducted using Ciprofloxacin as a positive control (275 µg/mL), and their results were compared to those obtained using an onion extract and DMSO as a negative control. Each plates zone of inhibition was quantified, and the experiment was run three times.

Preparation of culture strains

A nutrient broth subculture was used to create the pure cultures, which were then incubated at 37 °C overnight for 24 hrs. The cultures were diluted in the same broth until they had 10⁻³ cfu/mL of concentration. In order to produce the plates, 15 mL of nutritional agar, 1 mL of each diluted culture and the drilling of wells with sterile pipette tips were required. We moved and added 25 µL of each ZnO NP concentration (225, 250, 275, and 300 µg/mL) to the wells. After being left to stand for diffusion, the plates underwent a 24 hr incubation at 37 °C.

RESULTS AND DISCUSSION

XRD analysis

Fig. 1 displays the XRD pattern of fabricated ZnO NPs that was calcined at 400 °C for 2 hrs. Diffraction peaks were seen for lattice planes (100), (002), (101), (102), (110), (103), (200), (112), (200), and (201) at 31.61°, 34.19°, 36.11°, 47.32°, 56.49°, 62.67°, 65.85°, 67.77° and 68.9°, respectively. These peaks confirmed that the hexagonal wurtzite structure had formed with JCPDS card No. 01-079-0208^{28,29}. The additional diffraction peaks, which were observed at 24.48°, 28.76°, and 40.5°, are considered to be caused by the onion species. The average particle size of ZnO NPs was found to be 8.13 nm using Debye Scherrers equation, which is in agreement with the results of SEM and TEM³⁰. The values are shown in **Table 1**, and by comparing the d-spacing value with the standard value, all values were found to be Compatible with the literature reference data²⁹. The *c/a* values confirmed that the prepared NPs were crystalline in nature. The estimated values for *a* and *c* in **Table 1**, are agreement with the published values (*a* = 3.246 Å, *c* = 5.219 Å)²².

FT-IR analysis

Fig. 2 displays the FT-IR spectra of biosynthesised ZnO NPs using from onion extract. In **Fig. 2**, O–H_(S) stretching of the alcohol and phenol groups, N–H_(As) stretching of proteins, and adsorbed water³¹ all contribute to the peak at 3407 cm⁻¹. C–H_(As) asymmetric stretching is attributed to the peak at 2927 cm⁻¹. The characteristic peak at 1636 cm⁻¹ is due to the C=O vibrations in the onion extract, which may have helped the formation of ZnO NPs³². ZnO NPs shows similar peaks; but there are small differences in their positions and intensities. However the broad peak at 3319 cm⁻¹, which was previously found in plant extract, was related to O–H or N–H. The bands at 1055 cm⁻¹ represented the C–O_(As) stretching of the carboxylic acid and ester functional groups. The similarities between the spectra of ZnO NPs and onion extract indicated the existence of bioactive organic groups as reducing agents, which confirmed that these bioactive groups were responsible for the fabrication and stabilization of prepared nanoparticles^{33,34}. the new peak was observed at 567 cm⁻¹ according to Zn–O_(As) stretching vibration,^{35,36}.

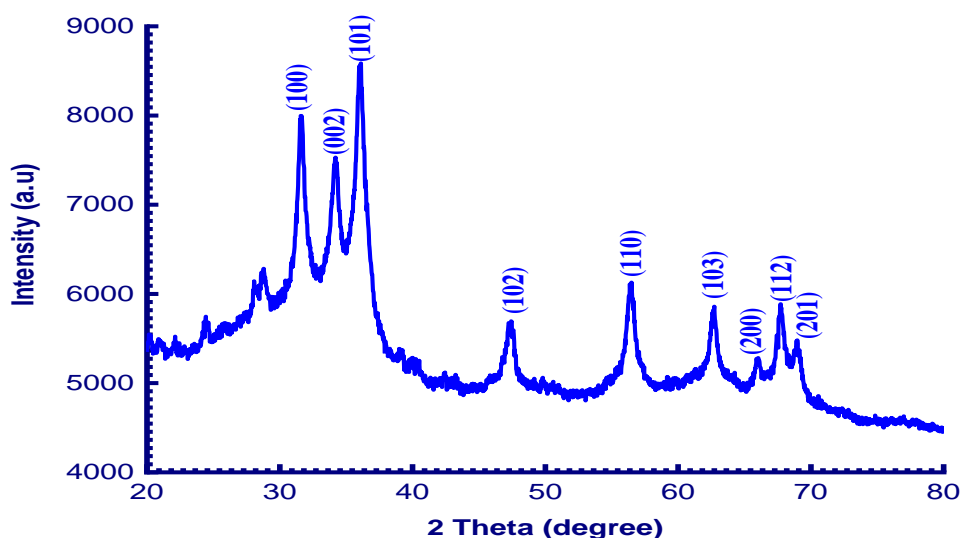


Fig. 1: X-ray diffractogram of biofabricated ZnO NPs.

Table 1: Comparison between XRD results of biosynthesized ZnO NPs and standard ZnO powder.

ZnO NPs	<i>a</i> (Å)	<i>c</i> (Å)	<i>v</i> (Å ³)	<i>c/a</i>	<i>D</i> ^x × 10 ⁴ (kg m ⁻³)
ZnO powder	3.264	5.219	48.17	1.598	6.213
ZnO NPs	3.2521	5.2221	47.83	1.604	6.214

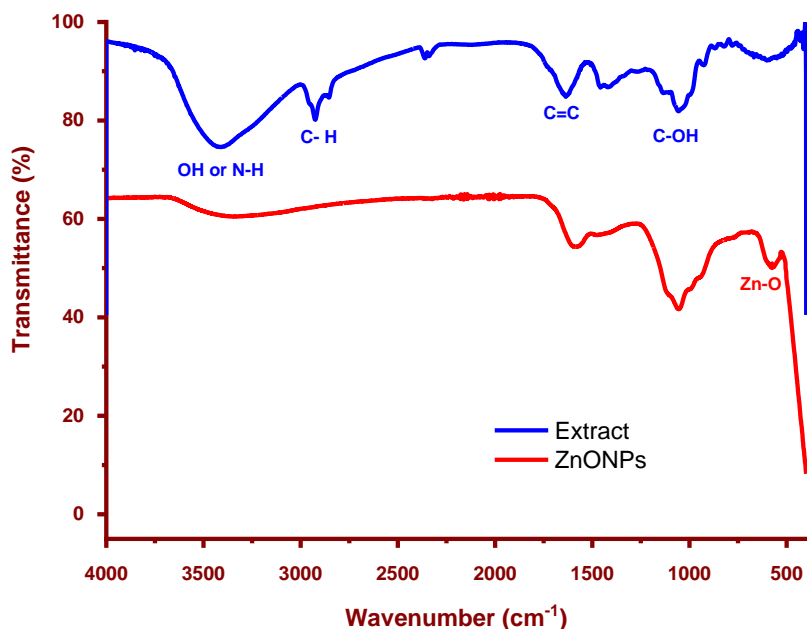


Fig. 2: FT-IR spectra of onion extract and as-biofabricated ZnO NPs.

Optical characteristics

Fig. 3 (a) displays the UV-visible spectrum of ZnO NPs dispersed in water. The ZnO NPs showed a single absorption peak at 374 nm, which is the characteristic peak for hexagonal wurtzite ZnO NPs and is almost identical to the ZnO NPs made by *Parthenium leaf*³⁷. When compared to the absorption peak of bulk ZnO (365 nm)³⁸, the peak exhibits a red shift of approximately 9 nm. The development of shallow levels can be the cause of this red shift. Additionally, no other peaks were visible in the spectrum, demonstrating the high purity of the prepared ZnO NPs. Employ equation 1 from the Tauc relationship to determine the semiconductors electronic band gap^{10,39}.

$$(\alpha h\nu)^n = A(h\nu - E_g) \quad (1)$$

where α is coefficient of absorption, h is the Planck's constant, ν is the photon frequency, and E_g is the optical band gap. The E_g in the direct transition was determined by extrapolating the linear portion of the plot of $(\alpha h\nu)^2$ against $h\nu$ (**Fig. 3(b)**), and it was found to be in the range (3.32 eV)^{9,40}. Evidently, from the estimated value of E_g for direct transition, the suggestion of the crystallinity nature of the biosynthesized ZnO NPs is confirmed. The photoluminescence spectrum analysis of as-synthesized ZnO NPs is shown in **Fig. 3(c)**. The explanation given for the blue-green

emission bands (excitonic transitions) seen at 428 nm was that the ZnO NPs had innate crystal defects⁴¹.

Morphology analysis (SEM, TEM and EDX analyses)

Fig. 4 displays the distribution curves (b & c), TEM and SEM microscopy (a & d) of fabricated ZnO NPs calcined at 400 °C for 2h. The spherical shape of the ZnO NPs is confirmed in **Fig. 4a** uniformly aggregated, and according to a study that examined the crystalline size of the generated NPs using TEM analysis, range in size from 2.06 to 15.35 nm on average. The ZnO NPs synthesized by onion extract were smaller than those previously reported⁴²⁻⁴⁵, according to the experiment analyses. The distribution curves show that the particle size of ZnO NPs ranges from 1 to 20 nm, and the average size is 9.01 nm (**Fig. 4b and c**). The EDX confirms the existence of zinc and oxygen signals in ZnO NPs, as seen in **Fig. 5**. The elemental composition of the biosynthesized ZnO NPs was determined using EDX analysis. The sample created using onion extract has pure ZnO phases, according to the energy dispersive spectra of the samples obtained from the SEM-EDX analysis. Analysis of the sample showed that they had wt% of the elements 71.33% Zn and 15.13 O, indicating that the produced ZnO NPs are in their purest form^{25,46}.

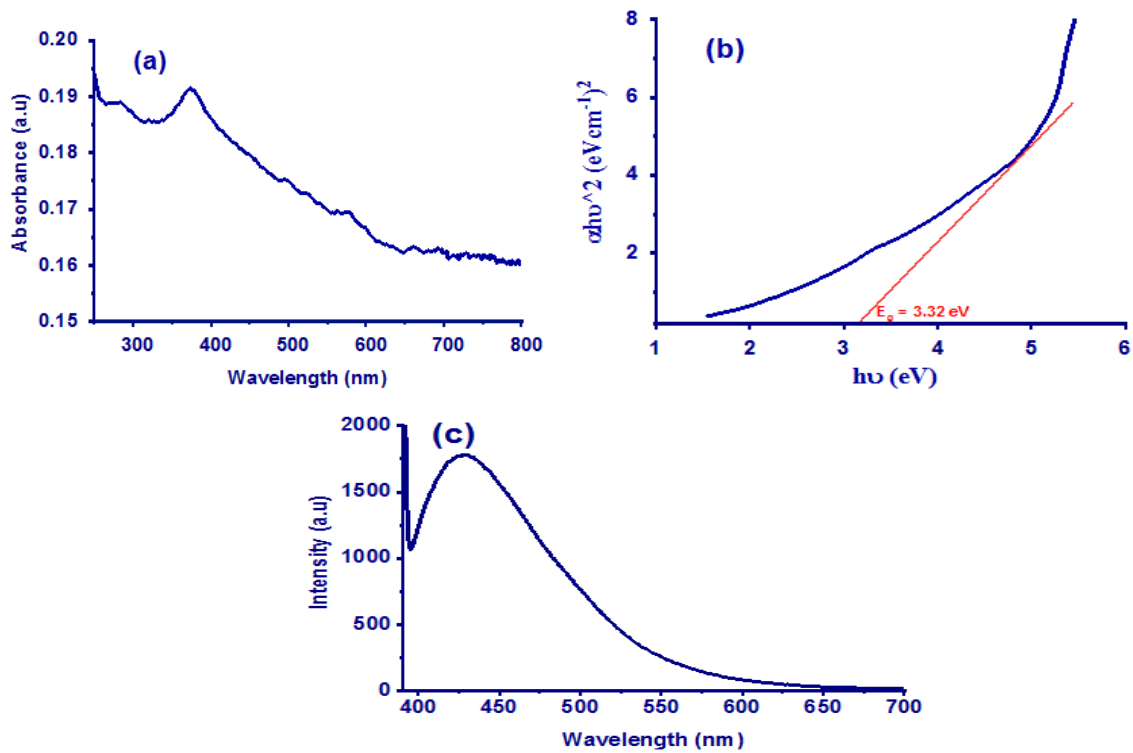


Fig. 3: UV-vis absorption (a), plots of $(\alpha h\nu)^2$ as a function of photon energy $h\nu$ for a direct bandgap (b), and PL spectra of fabricated ZnO NPs (c).

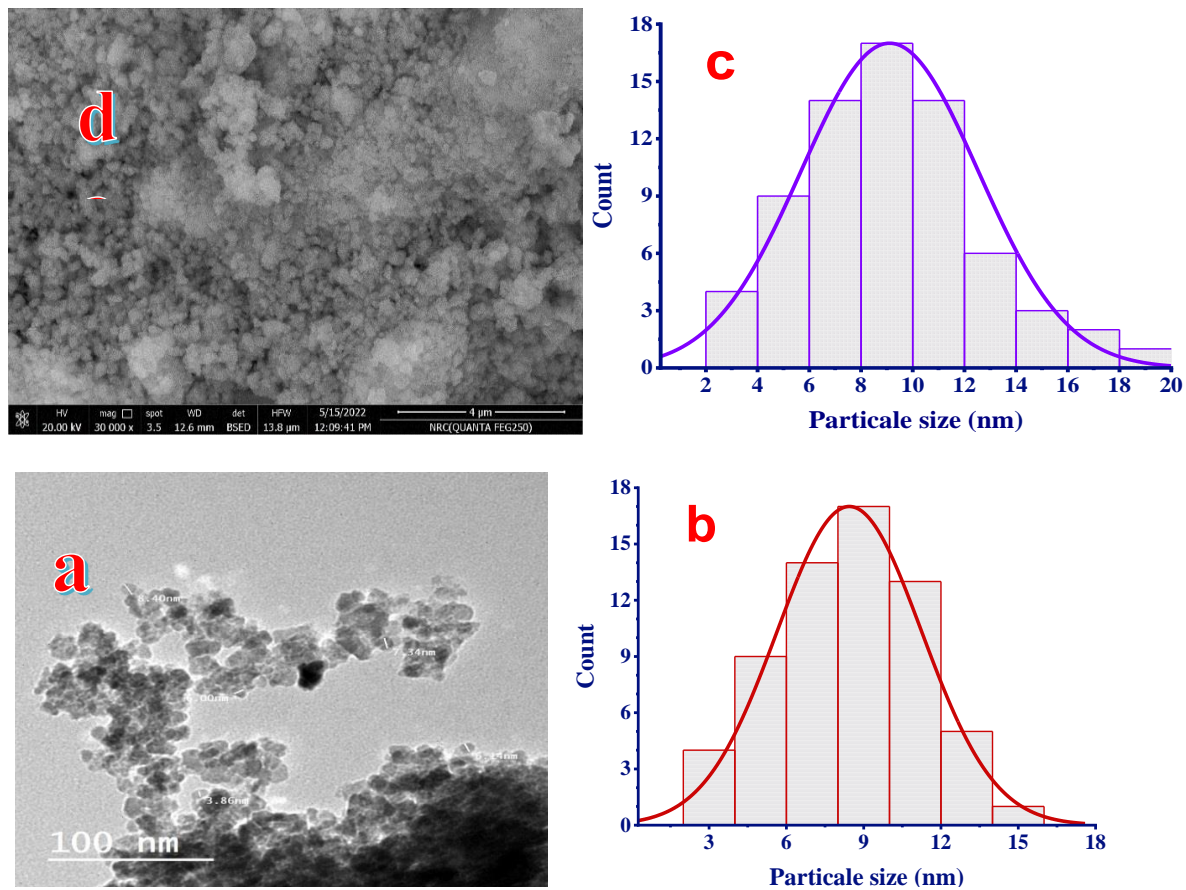


Fig. 4: Particle size distributions (b & c), TEM and SEM microscopy (a & d) of fabricated ZnO NPs.

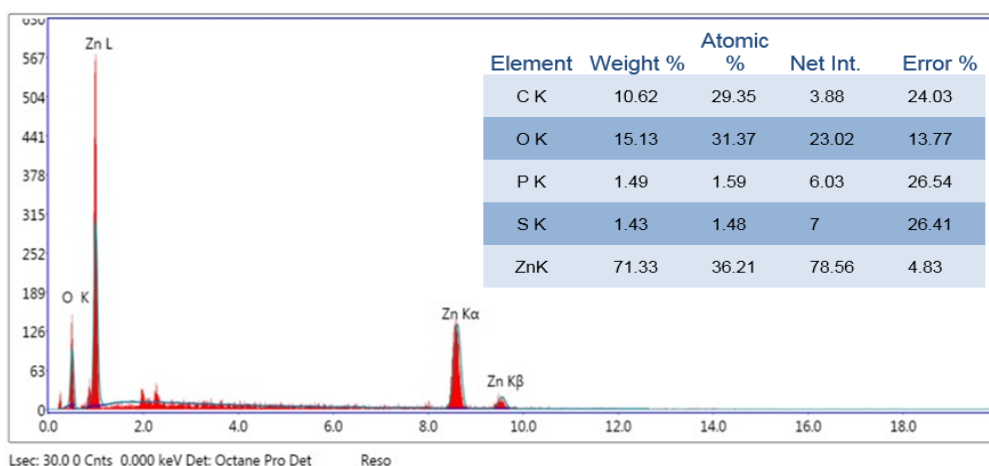


Fig. 5: EDX analysis of as-prepared ZnO NPs.

Raman analysis

ZnO NPs have a hexagonal wurtzite structure that is fit into the P63mc space group²². Only the optical phonons near the Brillouin zone's point Γ , participate in first-order Raman scattering for the perfect ZnO crystal. Equation 2 lists the optical modes that should be present in a wurtzite ZnO based on the group theory.

$$T_{opt} = A_1 + 2B_2 + E_1 + 2E_2 \quad (2)$$

where, both A_1 and E_1 modes are polar branches, split into a transverse optical mode (TO), and a longitudinal optical mode (LO). E_2 mode consists of low E_{γ}^{low} and high E_{γ}^{high} frequency phonons modes. E_{γ}^{low} is associated with the vibration of the oxygen atom and E_{γ}^{high} is related to heavy Zn sublattices⁴⁷. The first-

order Raman-active modes are A_1 , E_1 , and E_2 . Additionally, the B_1 modes, also known as silent modes are typically inactive in Raman spectra. **Fig. 6** shows the Raman spectra for the ZnO NPs, which had typical peaks in the 400–700 cm^{-1} range. One of the distinctive modes of the hexagonal wurtzite phase of ZnO, the high-frequency branch of the nonpolar optical phonon E_2^{high} of ZnO matched to the high-intensity peak seen at 446 cm^{-1} . The high-intensity peaks correlation with the E_2^{high} optical mode also emphasized the remarkable structural integrity and optical properties of the greenly synthesized ZnO NPs made from onion extract⁴⁸. The additional peaks at 613 and 628 cm^{-1} do not match up with ZnO normal modes. These peaks represent other vibrational modes linked to faults⁴⁹⁻⁵¹.

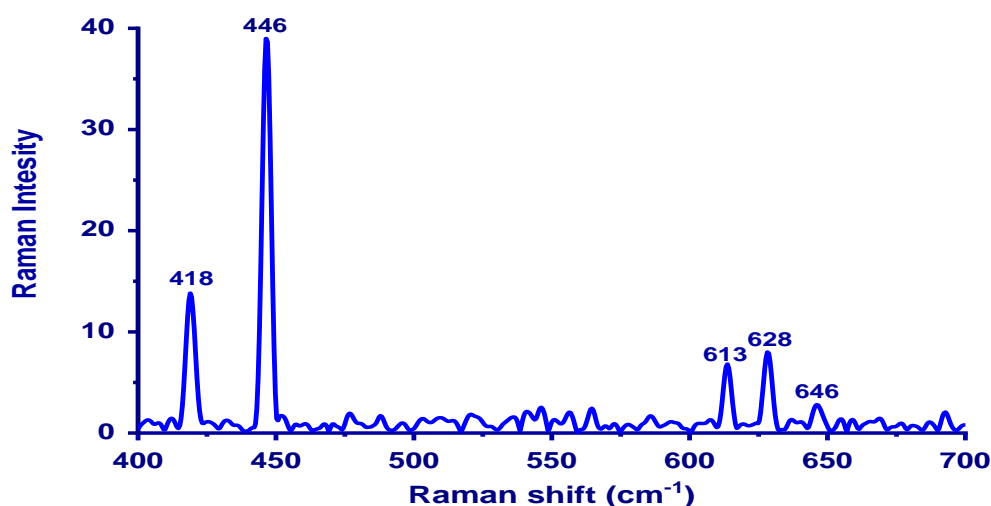


Fig. 6: Raman spectrum of biosynthesis ZnO NPs.

The antimicrobial activity of ZnO NPs

Minimum inhibitory concentration values were evaluated to study the antibacterial properties of the biosynthesis of ZnO NPs using red onion extract. The results are shown in Table 2 below. Following treatment with ZnO NPs at various concentrations 225, 250, 275, and 300 µg/mL against *S.typhimurium* and *E.coli*, *E.faecalis*, and *S.aureus*, the antibacterial activity demonstrated inhibitory zones (Gram-positive bacteria). Against both Gram-positive and Gram-negative bacteria, the ZnO NPs showed strong antibacterial action, according to the antibacterial activity results. *S. typhimurium*, *E. coli*, *S. aureus*, and *E. faecalis* growth inhibition has generally been increased by increasing the concentration of ZnO NPs. The zone of inhibition that ZnO NPs create against all different microbes is depicted in **Fig.s 7 and 8**. *E. coli* (MIC 31.2 ± 0.76 mm), *S. aureus* (MIC 30.2 ± 1.04 mm), *E. faecalis* (MIC 28.3 ± 0.76 mm), and *S. typhimurium* (MIC 26.3 ± 0.94 mm) were shown to be the species most sensitive to the nanoparticles.

Therefore, as compared to conventional antibiotics, ZnO NPs showed better antibacterial activity against gram-negative (*E. coli*) than gram-positive (*S. aureus*) bacteria. This is in line with earlier research that found ZnO NPs had a larger antibacterial effect on gram-negative bacteria than gram-positive bacteria⁵². However, it has been found that ZnO NPs have a stronger effect on gram-positive bacteria than gram-negative bacteria⁵³. This argument emphasises the significance of comprehending the mechanism underlying ZnO NPs antibacterial action⁵⁴. Additionally, the efficiency of the functional groups that helped produce ZnO NPs during their biogenesis. Previous studies have described the mechanism of ZnO NPs antimicrobial activity, and they claimed that ZnO NPs exhibit antimicrobial activity by damaging cell membranes as a result of direct or electrostatic contact between ZnO NPs and cell surfaces, cellular internalisation of ZnO NPs, and the production of active oxygen species like H₂O₂ in cells as a result of metal oxides^{53,55}.

Table 2: Evaluation the antibacterial activity of ZnO NPs (mean ± standard deviation; n = 3).

Microorganisms	Gram reactive	ZnO NPs	<i>Ciprofloxacin</i>
		25 µL from 250 µg/mL	25 µL from 275 µg/mL
Inhibition zone (mm)			
<i>E.coli</i>	- ve	31.2 ± 0.76	5.30 ± 0.50
<i>S.aureus</i>	+ ve	30.2 ± 1.04	30.3 ± 0.58
<i>E. faecalis</i>	+ ve	28.3 ± 0.76	28.1 ± 0.76
<i>S. typhimurium</i>	- ve	26.0 ± 0.94	30.6 ± 0.47

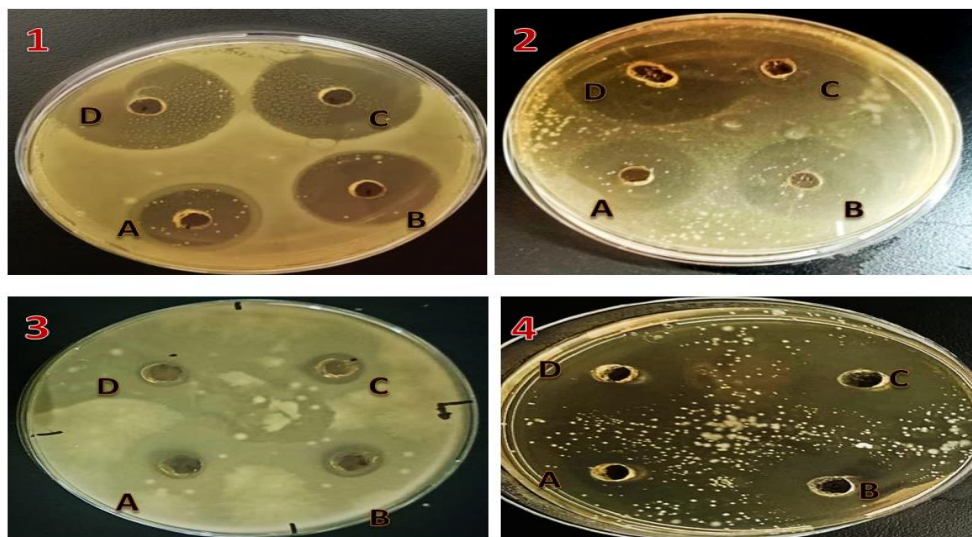


Fig. 7: Antimicrobial activity of ZnONPs solutions against; (1) *E.coli* (2) *S.aureus* (3) *E. faecalis* (4) *S. typhimurium* for representing bacteria. The concentration of solutions, A = 225, B = 250, C = 275, and D = 300 µg/mL.

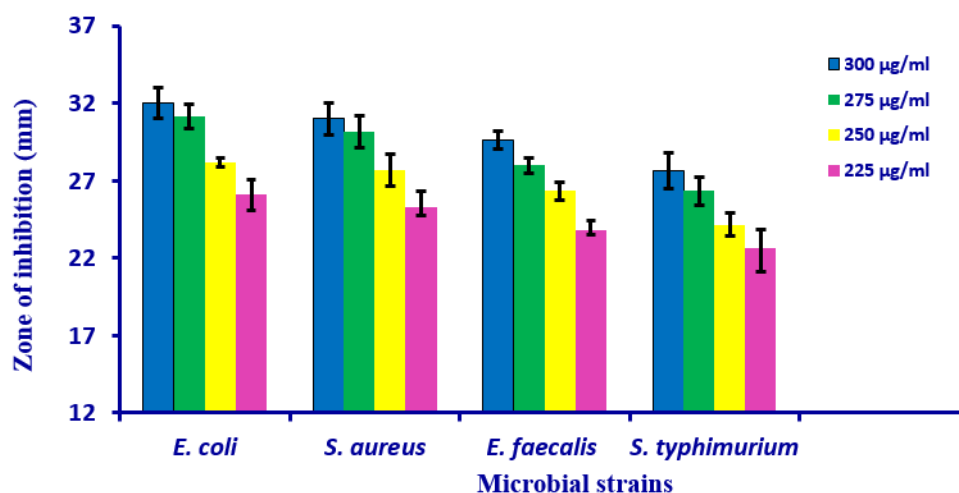


Fig. 8: Antibacterial activities of the biosynthesis ZnO NPs against *E.coli*, *S.aureus*, *E. faecalis*, and *S. typhimurium*.

Fig. 9 shows a comparison of 25 µL of (250 µg/mL) ZnO NPs, 25 µL of (275 µg/mL) *Ciprofloxacin*, DMSO, and onion extract. In the inhibition zone that was visible from each plate, the data demonstrated that the biosynthesized ZnO NPs worked better than the *Ciprofloxacin* employed as a positive control, but there was no inhibition zone in the controlled wells treated with red onion extract and DMSO. The highest inhibitory zone against *E.coli* and

S.aureus was seen, and it was followed by *E.faecalis* and *S.typhimurium*, showing that the bacteria were more averse to nanoparticle production. ZnO NPs may be more successful at inactivating a human infections than regular antibiotics, according to the antibacterial activity, which demonstrated that they are more harmful to bacterial cells.

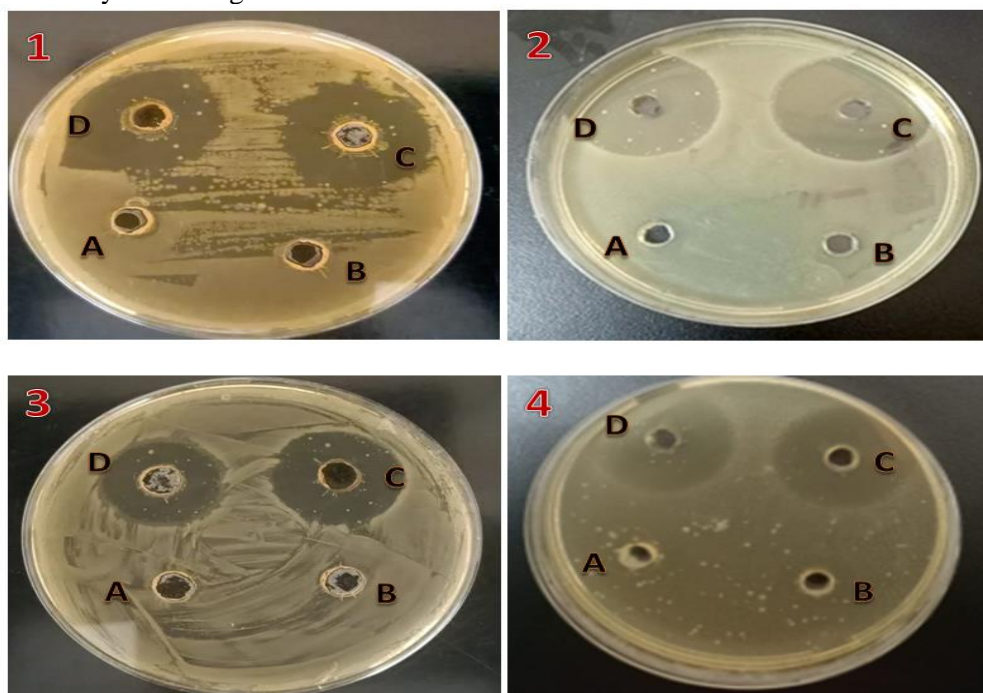


Fig. 9: Antimicrobial activity of 250 µg/mL ZnO NPs against (1) *E.coli* (2) *S. aureus* (3) *E. faecalis*, and *S. typhimurium* (4), the letters A, B, C, and D refer to DMSO and onion extract, 250 µg/mL ZnO NPs and 275 µg/mL of *Ciprofloxacin*, respectively.

Conclusions

The first demonstration of employing onion extract as a potent oxidizing/reducing chemical agent to create ZnO NPs, via a green, distinctive, and environmentally friendly process to create exceptionally crystalline ZnO NPs. XRD, UV-Vis spectroscopy, FTIR, Raman, SEM, EDX, and TEM were used to analyze ZnO NPs. The presence of the phytoconstituents in FT-IR analyses for both aqueous onion extract and ZnO NPs demonstrates their importance in the production of NPs. All of the recorded peak intensity profiles were determined to be the hexagonal wurtzite structure of ZnO NPs based on the XRD findings. The ZnO NPs possessed a spherical shape, a cluster of agglomerated particles, and a particle size range of 2.83-15.35 nm, per SEM and TEM studies. The EDX analysis verified the ZnO NPs elemental compositions. The bio-produced ZnO NPs were used as antibacterial materials as well. According to the antibacterial activity, the ZnO NPs examined to be more toxic to bacterial cells and may also be more effective at inactivating some human infections than the common drug Ciprofloxacin. The highest levels of inhibition were shown by *E. coli* and *S. aureus* after *E. faecalis* and *S. typhimurium*, demonstrating the selective action of ZnO on biological systems.

REFERENCES

1. H. Reinsch, "“Green” Synthesis of metal-organic frameworks", *Eur J Inorg Chem*, 2016(27), 4290-4299 (2016).
2. I. Ali, O. M. L. Alharbi, Z. A. Alothman, A. Y. Badjah, A. Alwarthan and A. A. Basheer, "Artificial neural network modelling of amido black dye sorption on iron composite nano material: Kinetics and thermodynamics studies", *J Mol Liq* 250, 1-8 (2018).
3. M. F. Al-Hakkani, G. A. Gouda, S. H. Hassan, M. Mohamed and A. M. Nagiub, "Environmentally azithromycin pharmaceutical wastewater management and synergetic biocompatible approaches of loaded azithromycin@hematite nanoparticles", *Sci Rep*, 12, 1-21 (2022).
4. M. F. Al-Hakkani, G. A. Gouda and S. H. Hassan, "A review of green methods for phyto-fabrication of hematite (α -Fe₂O₃) nanoparticles and their characterization, properties, and applications", *Heliyon*, 7, e05806 (2021).
5. M. F. Al-Hakkani, G. A. Gouda, S. H. Hassan, M. M. Mohamed and A. M. Nagiub, "Cefixime wastewater management via bioengineered Hematite nanoparticles and the in-vitro synergetic potential multifunction activities of Cefixime@ Hematite nanosystem", *Surf Interfaces*, 30, 101877 (2022).
6. E. H. Elshazly, A. Nasr, M. E. Elnosary, G. A. Gouda, H. Mohamed and Y. Song, "Identifying the Anti-MERS-CoV and Anti-HcoV-229E Potential Drugs from the Ginkgo biloba Leaves Extract and Its Eco-Friendly Synthesis of Silver Nanoparticles", *Molecules*, 28(3), 1375 (2023).
7. Z. Chu, T. Zhao, L. Li, J. Fan and Y. Qin, "Characterization of antimicrobial poly (lactic acid)/nano-composite films with silver and zinc oxide nanoparticles", *Materials* 10(6), 659 (2017).
8. S. Hosny, G. A. Gouda and S. M. Abu-El-Wafa, "Novel nano copper complexes of a new Schiff base: Green synthesis, a new series of solid Cr (II), Co (II), Cu (II), Pd (II) and Cd (II) chelates, characterization, DFT, DNA, antitumor and molecular docking studies", *Appl Organomet Chem*, 36(5), e6627 (2022).
9. E. H. Elshazly, A. K. S. Mohamed, H. A. Aboelmagd, G. A. Gouda, M. H. Abdallah, E. A. Ewais *et al.*, "Phytotoxicity and Antimicrobial Activity of Green Synthesized Silver Nanoparticles Using Nigella sativa Seeds on Wheat Seedlings", *J Chem*, 2022, Article ID 9609559 (2022).
10. E. Hassan, A. A. Gahlan and G. A. Gouda, "Biosynthesis approach of copper nanoparticles, physicochemical characterization, cefixime wastewater treatment, and antibacterial activities", *BMC Chem* 17, 1-20 (2023).
11. K. Gopinath, V. Karthika, S. Gowri, V. Senthilkumar, S. Kumaresan and A. Arumugam, "Antibacterial activity of ruthenium nanoparticles synthesized using

- Gloriosa superba L. leaf extract", *J Nanostruct Chem*, 4(1), 83 (2014).
12. A. K. Mittal, Y. Chisti and U. C. Banerjee, "Synthesis of metallic nanoparticles using plant extracts", *Biotechnol Adv*, 31(2), 346-356 (2013).
 13. S. Irvani, "Green synthesis of metal nanoparticles using plants", *Green Chem*, 13(10), 2638-2650 (2011).
 14. A. A. Aly, A. H. Osman, M. A. El-Mottaleb and G. A. Gouda, "Reactivity of certain biologically important Azoles and morpholine towards Ni (II) and Cu (II) complexes of o-hydroxyacetophenoneethanolimine and N-Salicylidene derivatives", *Bulletin of Pharmaceutical Sciences. Assiut*, 29(1), 134-149 (2006).
 15. S. Sarkar, N. T. Ponce, A. Banerjee, R. Bandopadhyay, S. Rajendran and E. Lichtfouse, "Green polymeric nanomaterials for the photocatalytic degradation of dyes: a review", *Environ Chem Lett*, 18, 1569-1580 (2020).
 16. R. Hassaniien, D. Z. Husein and M. Khamis, "Novel green route to synthesize cadmium oxide@graphene nanocomposite: optical properties and antimicrobial activity", *Mater Res Express*, 6(8), 085094 (2019).
 17. F. J. Moreno, M. Corzo-Marti, M. D. Del Castillo and M. Villamiel, "Changes in antioxidant activity of dehydrated onion and garlic during storage", *Food Res Int*, 39(8), 891-897 (2006).
 18. X. Lu, J. Wang, H. M. Al-Qadiri, C. F. Ross, J. R. Powers, J. Tang, *et al.*, "Determination of total phenolic content and antioxidant capacity of onion (*Allium cepa*) and shallot (*Allium oschaninii*) using infrared spectroscopy", *Food Chem*, 129(2), 637-644 (2011).
 19. J. Osuntokun, D. C. Onwudiwe and E. E. Ebenso, "Green synthesis of ZnO nanoparticles using aqueous *Brassica oleracea* L. var. *italica* and the photocatalytic activity", *Green Chem Lett Rev* 12(4), 444 - 457 (2019).
 20. Z.-Y. Zhang and H.-M. Xiong, "Photoluminescent ZnO nanoparticles and their biological applications", *Materials*, 8(6), 3101-3127 (2015).
 21. R. Shashanka, H. Esgin, V. M. Yilmaz and Y. Caglar, "Fabrication and characterization of green synthesized ZnO nanoparticle based dye-sensitized solar cells", *J Sci Adv Mater Devices*, 5(2), 185-191 (2020).
 22. M. Ameri, M. Raoufi, M.-R. Zamani-Meymian, F. Samavat, M.-R. Fathollahi and E. Mohajerani, "Self-assembled ZnO nanosheet-based spherical structure as photoanode in dye-sensitized solar cells", *J Electron Mater*, 47, 1993-1999 (2018).
 23. M.-R. Zamani-Meymian, N. Naderi and M. Zareshahi, "Improved n-ZnO nanorods/p-Si heterojunction solar cells with graphene incorporation", *Ceramics International* 48(23 Part A), 34948-34956 (2022).
 24. T. A. Singh, J. Das and P. C. Sil, "Zinc oxide nanoparticles: A comprehensive review on its synthesis, anticancer and drug delivery applications as well as health risks", *Adv Colloid Interface Sci*, 286, 102317 (2020).
 25. M. Khamis, G. A. Gouda, A. M. Nagiub, "Biosynthesis approach of zinc oxide nanoparticles for aqueous phosphorous removal: physicochemical properties and antibacterial activities", *BMC Chemistry* 17, 99 (2023).
 26. A. Patterson, "The Scherrer formula for X-ray particle size determination", *Phys Rev*, 56(10), 978 (1939).
 27. H. M. Al-Saidi, G. A. Gouda, M. Abdel-Hakim, N. I. Alsenani, A. Alfarsi, M. H. Mahross, *et al.*, "Synthesis and Characterization of Ni (II), Cu (II), Zn (II) and Azo Dye Based on 1, 10-o-Phenanthroline Binary Complexes: Corrosion Inhibition Properties and Computational Studies", *Int J Electrochem Sci*, 17(3), 220333 (2022).
 28. R. Wahab, I. Hwang, Y.-S. Kim, J. Musarrat, M. Siddiqui, H.-K. Seo, *et al.*, "Non-hydrolytic synthesis and photocatalytic studies of ZnO nanoparticles", *Chem Eng J* 175, 450-457 (2011).
 29. N. Srinivasan and J. C. Kannan, "Investigation on room temperature photoluminescence of pure and aluminum doped zinc oxide nanoparticles", *Mater Sci-Pol*, 33(1), 205-212 (2015).

30. Q. I. Rahman, M. Ahmad, S. K. Misra and M. Lohani, "Effective photocatalytic degradation of rhodamine B dye by ZnO nanoparticles", *Mater Lett*, 91, 170-174 (2013).
31. B. S. Al-Farhan, G. A. Gouda, O. Farghaly and A. El Khalafawy, "Potentiometric study of new Schiff base complexes bearing morpholine in ethanol-water medium with some metal ions", *Int J Electrochem Sci*, 14, 3350-3362 (2019).
32. A. Jayachandran, T. Aswathy and A. S. Nair, "Green synthesis and characterization of zinc oxide nanoparticles using Cayratia pedata leaf extract", *Biochem Biophys Rep*, 26, 100995 (2021).
33. A. H. Osman, A. A. Aly, M. A. El-Mottaleb and G. A. Gouda, "Photoreactivity and thermogravimetry of copper (II) complexes of N-salicylideneaniline and its derivatives", *Bull Korean Chem Soc*, 25, 45-50 (2004).
34. T. Varadavenkatesan, E. Lyubchik, S. Pai, A. Pugazhendhi, R. Vinayagam and R. Selvaraj, "Photocatalytic degradation of Rhodamine B by zinc oxide nanoparticles synthesized using the leaf extract of Cyanometra ramiflora", *J Photochem Photobiol B*, 199, 111621 (2019).
35. R. Hassan, A. Gahlan, G. A. Gouda, M. A.-E. Aly-Eldeen and N. Badawy, "Development of zinc removal process from contaminated water using statistical approaches", *Egypt J Chem*, 65(131), 1099-1110 (2022).
36. A. S. Abdulhadi, G. A. Gouda, A. M. Hamed, M. Abu-Saied and M. El-Mottaleb, "Synthesis of ZnO Nano Powders Using Polyethylene Glycol By The Controlled Microwave Method", *Bull Pharmaceut Sci Assiut*, 45(1), 23-40 (2022).
37. P. Rajiv, S. Rajeshwari and R. Venkatesh, "Bio-Fabrication of zinc oxide nanoparticles using leaf extract of Parthenium hysterophorus L. and its size-dependent antifungal activity against plant fungal pathogens", *Spectrochim Acta Part A*, 112, 384-387 (2013).
38. M. Pudukudy and Z. Yaakob, "Facile synthesis of quasi spherical ZnO nanoparticles with excellent photocatalytic activity", *J Cluster Sci*, 26, 1187-1201 (2015).
39. P. Ramesh, K. Saravanan, P. Manogar, J. Johnson, E. Vinoth and M. Mayakannan, "Green synthesis and characterization of biocompatible zinc oxide nanoparticles and evaluation of its antibacterial potential", *Sens Bio-Sens Res*, 31, 100399 (2021).
40. Z. Durmus, B. Z. Kurt and A. Durmus, "Synthesis and characterization of graphene oxide/zinc oxide (GO/ZnO) nanocomposite and its utilization for photocatalytic degradation of basic fuchsin dye", *Chem Select*, 4(1), 271-278 (2019).
41. A.-S. Gadallah and M. El-Nahass, "Structural, optical constants and photoluminescence of ZnO thin films grown by sol-gel spin coating", *Adv Condens Matter Phys*, 2013, Article ID 234546 (2013).
42. E. Shayegan Mehr, M. Sorbiun, A. Ramazani and S. Taghavi Fardood, "Plant-mediated synthesis of zinc oxide and copper oxide nanoparticles by using ferulago angulata (schlecht) boiss extract and comparison of their photocatalytic degradation of Rhodamine B (RhB) under visible light irradiation", *J Mater Sci Mater Electron*, 29, 1333-1340 (2018).
43. H. Madan, S. Sharma, D. Suresh, Y. Vidya, H. Nagabhushana, H. Rajanaik, *et al.*, "Facile green fabrication of nanostructure ZnO plates, bullets, flower, prismatic tip, closed pine cone: their antibacterial, antioxidant, photoluminescent and photocatalytic properties", *Spectrochim Acta Part A*, 152, 404-416 (2016).
44. M. H. Kahsay, A. Tadesse, D. RamaDevi, N. Belachew and K. Basavaiah, "Green synthesis of zinc oxide nanostructures and investigation of their photocatalytic and bactericidal applications", *RSC Advances*, 9, 36967-36981 (2019).
45. S. Pal, S. Mondal, J. Maity and R. Mukherjee, "Synthesis and characterization of ZnO nanoparticles using Moringa oleifera leaf extract: investigation of photocatalytic and

- antibacterial activity", *Int J Nanosci Nanotechnol* 14(2), 111-119 (2018).
46. K. Dulta, G. Koşarsoy Ağçeli, P. Chauhan, R. Jasrotia, P. Chauhan, "Ecofriendly Synthesis of Zinc Oxide Nanoparticles by Carica papaya leaf extract and their applications", *J Cluster Sci* 33, 603-617 (2022).
 47. I. Musa, N. Qamhieh and S. T. Mahmoud, "Synthesis and length dependent photoluminescence property of zinc oxide nanorods", *Results in Physics*, 7, 3552-3556 (2017).
 48. K. Rambabu, G. Bharath, F. Banat and P. L. Show, "Green synthesis of zinc oxide nanoparticles using Phoenix dactylifera waste as bioreductant for effective dye degradation and antibacterial performance in wastewater treatment", *J Hazard Mater*, 402, 123560 (2021).
 49. D. Montenegro, V. Hortelano, O. Martínez, M. Martínez-Tomas, V. Sallet, V. Muñoz-Sanjosé, *et al.*, "Non-radiative recombination centres in catalyst-free ZnO nanorods grown by atmospheric-metal organic chemical vapour deposition", *J Phys D Appl Phys*, 46, 235302 (2013).
 50. M. F. Al-Hakkani, G. A. Gouda, S. H. Hassan and A. M. Nagiub, "Echinacea purpurea mediated hematite nanoparticles (α -HNPs) biofabrication, characterization, physicochemical properties, and its in-vitro biocompatibility evaluation", *Surf Interfaces*, 24, 101113 (2021).
 51. M. F. Al-Hakkani, G. A. Gouda, S. H. Hassan, M. S. Saddik, M. A. El-Mokhtar, M. A. Ibrahim, *et al.*, "Cefotaxime removal enhancement via bio-nanophotocatalyst α -Fe₂O₃ using photocatalytic degradation technique and its echo-biomedical applications", *Sci Rep*, 11881, 1-20 (2022).
 52. M. Shaban, F. Mohamed and S. Abdallah, "Production and characterization of superhydrophobic and antibacterial coated fabrics utilizing ZnO nanocatalyst", *Sci Rep*, 8, 1-15 (2018).
 53. K. Elumalai, S. Velmurugan, S. Ravi, V. Kathiravan and G. A. Raj, "Bio-approach: Plant mediated synthesis of ZnO nanoparticles and their catalytic reduction of methylene blue and antimicrobial activity", *Adv Powder Technol*, 26(6), 1639-1651 (2015).
 54. B. Lallo da Silva, M. P. Abuçafy, E. Berbel Manaia, J. A. Oshiro Junior, B. G. Chiari-Andréo, R. C. R. Pietro, *et al.*, "Relationship between structure and antimicrobial activity of zinc oxide nanoparticles: An overview", *Int J Nanomed*, 14(2019), 9395-9410 (2019).
 55. K. Karthik, S. Dhanuskodi, C. Gobinath and S. Sivaramakrishnan, "Microwave-assisted synthesis of CdO-ZnO nanocomposite and its antibacterial activity against human pathogens", *Spectrochim Acta Part A*, 139, 7-12 (2015).



نشرة العلوم الصيدلانية جامعة أسيوط



التخليق الحيوي لجسيمات أكسيد الزنك النانوية بواسطة مستخلص البصل الأحمر (Allium cepa) والنشاط المضاد للبكتيريا

مني خميس محمد - جمال عبدالعزيز جودة* - أدهم محمد نجيب

قسم الكيمياء ، كلية العلوم ، جامعة الأزهر بأسسيوط

الهدف الرئيسي من البحث هو تحضير جسيمات أكسيد الزنك النانوية ZnO NPs باستخدام مستخلص البصل الأحمر (Allium cepa) بواسطة التخليق الأخضر . متوسط الحجم بلوري في حدود ٨,١٣ نانومتر ، تم استخدام تقنية حيود الأشعة السينية (XRD) لتحديد الهيكل السداسي (Wurtzite) لجسيمات ZnO NPs. أكدت نتائج تحاليل الأشعة تحت الحمراء (FT-IR) تغطية واستقرار الجسيمات المتكونة حيويًا. تم تحديد قمة الامتصاص المميز لجسيمات أكسيد الزنك النانوية عند طول موجي ٣٧٤ نانومتر مع فجوة طاقة قدرها ٣,٣٢ إلكترون فولت بواسطة التحليل المرئي للأشعة فوق البنفسجية. تم إجراء التحليل المورفولوجي ، وأظهرت النتائج تكوين ZnO NPs بأشكالها الكروية وأحجام تتراوح من ٢,٨٣ إلى ١٥,٣٥ نانومتر. تم تحديد درجة النقاء والشدة والعرض البلوري للزنك والأكسجين بواسطة تحليل SEM-EDS. أظهر ZnO NPs تأثيرًا مضادًا للبكتيريا ضد الإيشيرشيا كولاي أكثر من بكتيريا الإستافيلوكوكس ، عند مقارنتها بمضاد حيوي شائع مثل سيبروفلوكساسين والذي تم استخدامه كعنصر تحكم إيجابي في المنطقة المثبطة ، وتم دراسة تأثير مستخلص البصل و DMSO ضد الأنواع المختلفة للبكتيريا و لكن هذه الإضافات لم تنتج منطقة مثبطة يمكن رؤيتها.